AN ECONOMETRIC MODEL OF FLIGHT EN ROUTE INEFFICIENCY

Yulin Liu
National Center of Excellence for Aviation Operations Research (NEXTOR II)
107D McLaughlin Hall
University of California, Berkeley, CA 94720
Tel: 510-590-7867; Email: liuyulin101@berkeley.edu

Mark Hansen
National Center of Excellence for Aviation Operations Research (NEXTOR II)
114 McLaughlin Hall
University of California, Berkeley, CA 94720
Tel: 510-642-2880; Fax: 510-643-3955; Email: mhansen@ce.berkeley.edu

Word count: 3648 words (in text) + 12 tables/figures x 250 words (each) = 6648 words

Submission Date: 08/01/2018

ABSTRACT

The Federal Aviation Administration (FAA) and Eurocontrol publish metrics to evaluate flight horizontal en route inefficiency (HIE), which measures the excess distance flown with respect to the theoretical shortest distance route. Knowledge of the factors that drive variation in en route efficiency is, however, limited. This paper proposes an approach to relate HIE with convective weather, wind, Miles-In-Trail restrictions (MIT), Airspace Flow Programs (AFP), Monitor Alerts (MA), and Special Activity Airspace (SAA). Furthermore, we develop econometric models to quantify how these factors affect HIE based on a historical dataset with flights among 97 major US airport pairs in 2013. Our analysis is based on the concept of a synthetic nominal route, in our case a great circle route, whose features are time-dependent, and are assumed to affect HIE of a given flight even though its trajectory does not follow the great circle. In the models, we also consider the effects of airspace route structure by inclusion of airport-pair fixed effects, and a measure of flight distance that is sensitive to the efficient placement of terminal entry and exit points. The estimation results suggest that long-haul flights are in general more efficient than short-haul flights, and inefficient terminal entry and exit points lead to greater HIE. The estimates confirm that inefficiency is greater when synthetic great circle routes have greater exposure to convective weather, unfavorable winds, MITs, SAAs, and long-delay AFPs. Finally, we find that MAs do not appear to have much direct impact on en route inefficiency.

Keywords: En route inefficiency, convective weather, wind, Miles-In-Trail, Airspace Flow Program, Special Activity Airspace, Monitor Alert; Fixed effects model

1. INTRODUCTION

In recent years, flight en route performance has received more attentions in the literature. In both US and Europe, it is evaluated by a simple metric termed as "horizontal en route inefficiency" (HIE), which is calculated based on the actual distance traveled and a benchmark distance between a 40 nautical-mile circular boundary around the departure airport (D40) and a 100 nautical-mile circular boundary around the arrival airport (A100). Equation 1 formulates the HIE, where A is the actual flown distance, and H is the benchmark distance termed as the "achieved distance" *(1)*. While the achieved distance is highly correlated with the D40A100 great circle distance, it captures the effects of terminal exit and entry points and varies from flight to flight.

$$HIE = \frac{A-H}{H} \quad (1)$$

Simple as it is, flight en route inefficiency is core to many fuel efficiency benefit assessments. Therefore, both the Federal Aviation Administration (FAA) and Eurocontrol employ the metric and publish joint annual report to compare and evaluate the overall performance in both regions. Ref. *(2)* reports that in 2013, the HIE was 2.91% and 2.71% for Europe and the US, respectively. With the implementation of free route airspace (FRA), Europe experienced continuous improvement of HIE between 2011 and 2014, however, this trend reversed in 2015. US HIE improved from 2008 to 2012, but has been worsened since then. This has been linked to airports with increased traffic levels (LAX, SEA, DAL) *(2)*. However, work on linking inefficiencies to specific causal reasons, a necessary step in developing strategies to improved performance, is limited. Accordingly, in this study, we will identify potential causal factors and the mechanisms by which they may contribute to HIE, propose metrics that quantify the exposure of individual flights to these factors, and, lastly, build econometric models to quantify the effects of different factors on HIE.

The rest of the paper is organized as follows. In section 2, we first review literature that is related to en route inefficiency analysis, and then introduce the datasets used in the study. Section 3 describes the methodology and algorithms of the paper. Section 4 presents the results and our analysis, and section 5 offers the conclusions.

2. PRELIMINARIES

2.1 Literature Review

There is some previous literature analyzing correlations between different causal factors and flight en route inefficiency. Liu et al. (2017) examine the causal effects of weather, wind and Miles-In-Trail (MIT) restrictions on en route inefficiency using the concept of nominal routes *(3)*. In the paper, the authors select six airport pairs and build airport-pair specific models to quantify the contributions of different factors. The results vary across pairs but in general convective weather has the greatest contribution, followed by wind and miles-in-trail restrictions. However, the factors considered in that study together account for a small fraction of the total en route efficiency. In part, this is because the study considers factors that vary from flight to flight for a given airport pair. Therefore, the present study adopts a different approach: we estimate pooled cross-sectional models that are informed by HIE variation both within and between different airport pairs. This allows us to investigate factors whose variation is substantially between pairs rather than between flights within a pair, such as special activity airspace (SAA) and airspace flow programs. Moreover,

the methodology adopted here is more readily "scalable" so that much larger number of airport pairs can be incorporated into the analysis.

One set of factors that affect HIE pertains to weather – including convective weather and winds. There is extensive literature on modeling flight trajectories in avoidance of convective weather. For example, McNally et al. (2012) and McNally et al. (2013) developed tools to automatically reroute flights to find more efficient routes around convective weather, which they termed "dynamic weather routes" *(4)*, *(5)*. Flights almost will always go around hazardous weather zones (see SWAP from *(6)*) and therefore increase their HIE. Additionally, a large body of literature focuses on optimizing trajectories with respect to wind – i.e. finding the wind optimal route *(7)*, *(8)*, *(9)*. In many cases, a flight taking the great circle trajectory, which is the shortest path, will not be optimal when winds are taken into account. Therefore, a flight that is "inefficient" in terms of HIE flight may actually be more "efficient" in terms of fuel/flight time.

Another important group of potential factors contributing to HIE is traffic management initiatives (TMIs), particularly those related to airspace. They have received far less attention in the open literature. One such initiative is Miles-In-Trail restrictions (MIT), which specify the minimal distance required between two consecutive aircrafts over a fix, airport, sector or route *(6)*. MITs are a common tool that FAA uses to maintain a manageable flow into busy airspace. Ref. *(10)* reports that MIT restrictions did not have significant effects on airborne delay, but their effect on HIE has only been studied recently. Liu et al. (2017) reports that MITs have a statistically significant impact for certain pairs such as JFK to FLL *(3)*. However, how and to what degree MIT may affect the traffic flow and flight inefficiency in a broader range of airport pairs need further exploration. A second example is Airspace Flow Programs (AFP), which identify constrained areas in the airspace and assign expected departure clearance times (EDCT) to flights entering the area. Flights can choose either stay in the AFP and accept the EDCT and its attendant ground delay, or reroute the flight out of AFP to get a longer route, or reroute to another AFP with lower expected delays. Tereshchenko and Hansen (2018) studied the airline decision making in response to the AFP with emphasis of relative trajectory costs. Though the authors conclude that flights usually avoid rerouting out of AFP, but such reroutes are common enough so that AFPs could affect en route inefficiency *(11)*. Thirdly, Special Activity Airspace (SAA) defines 3D geometries in the NAS wherein limitations are imposed on aircraft operations at certain times, when the SAA is said to be "active." SAAs include Special Use Airspace (SUA) such as Military Operational Areas (MOA), Restricted Areas (RA) and Air Traffic Control Assigned Areas (ATCAA). SAA activation and de-activation involves communication and negotiation between FAA and DoD, but lacks flexibility and automation *(12)*. Krozel et al. (2008) designed tools to balance the usage of SAA between military and civilian operations. The authors point out that up to the publication date, the dispatchers must assume that aircraft will have to fly around all known SUAs regardless the active status and must be fueled to do so *(13)*. Therefore, a system by which the military can activate SUAs based on its needs and civilian airspace users can use unused SUAs would be of great benefit. The data used in our study confirm that most flight trajectories deliberately avoid the SUA areas, even if they are not activated. Lastly, Monitor Alert (MA) is a tool that alerts sector personnel when the forecast flight demand exceeds Monitor Alert Parameter (MAP) value, which is an indicator of sector capacity. When the forecast demand, which is based on the number of flights that have already departed in a given time interval, exceeds the MAP value, MA will be triggered as "red" alert; otherwise, it will be triggered as "yellow" alert.. Sector personnel receiving the alert

must evaluate the impact and take appropriate actions *(14)*. Actions include but not limited to accepting traffic, splitting the sector, and requesting TMIs such as MIT and AFP. While not a TMI per se, MA's may also affect HIE if flights are rerouted to avoid the red or yellow regions.

2.2 Data Sources and Summary Statistics

In this study, we combined eight historical datasets from different sources. The flight event dataset, which comes from the Traffic Flow Management System (TFMS) of the FAA, contain the flight level en route performance statistics including D40 – A100 actual flown distance and D40 – A100 achieved distance. We obtained the data for the calendar year (CY) 2013 and derived the flight en route inefficiency. The full dataset includes around 6.5 million records, 87% of which are domestic flights. In this study, we limit our scope to flights among the US main 34 airports listed in the 2013 US-Europe operational performance report, which accounts for around 47% of the total traffic with an average en route inefficiency of 3.41%.

The flight tracks dataset, which also comes from the FAA TFMS, contains the 4D position – longitude (in degrees), latitude (in degrees), altitude (in 100 feet), and time (in seconds) – for each flight throughout its trip. The time resolution of the flight tracks is typically 1 minute. In this study, we first sampled 97 airport pairs based on the traffic volume in the flight event dataset and then queried into the TFMS to obtain all flight tracks among the selected pairs in CY2013. Figure 1 shows the selected airport pairs. The red markers are selected airports, and the green curves are great circle routes connecting any two airports. After preprocessing all the flight tracks, we ended up with 436,830 flights in 2013.

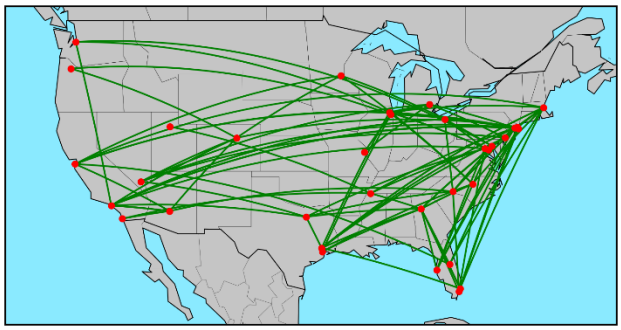

Figure 1 Selected airport pairs (direction not specified in the figure)

We derived the convective weather data from the Quality Controlled Local Climatological Data (QCLCD). The dataset includes hourly summaries for different weather instances, such as thunderstorm, rain, hail, etc., at around 2,500 ground stations in the US. Each record is a vector of binary variables indicating whether there was a certain type of weather instance occurring at a specific time and location. We collected the weather data in CY2013.

The wind dataset, which comes from the National Center for Atmospheric Research (NCAR), contains raster of southerly and westerly wind speeds at specific hours and grid points. To be more specific, the dataset records the wind speed four times a time – 00:00, 06:00, 12:00, 18:00 UTC – and each grid point is described as a tuple of (longitude, latitude, pressure altitude). The horizontal grid resolution is $2.5° \times 2.5°$, and there are 17 pressure levels ranging from 10 mbar (around

85,000 ft) to 1000 mbar (around 350 ft). For CY2013, we ended up with 1,460 raster files.

The Miles-In-Trail (MIT), Airspace Flow Program (AFP), and Monitor Alert (MA) datasets all come from the National Traffic Management Log (NTML). The MIT data describe where, when, why and how the MIT restrictions were implemented. Fields of interest include: requesting facility (center), providing facility (center), NAS element (where the MIT was initiated), time and spacing parameters. The AFP dataset records, similar to MIT, when and where the AFP was initiated, and what the assigned flight delay and acceptance rate were. Interested readers may also refer to the AFP visualizer web tool developed by Estes *(15)*. Since both MITs and AFPs are often modified, extended or cancelled after initiation, we excluded those MITs or AFPs that were cancelled before initiation, and merged those that were extended or modified from the initial plan. The monitor alert, while is a tool that reflects the projected demand in different sectors, was recorded in the MA dataset by the alert time, alert type and the corresponding actions. We collected all the three datasets for CY2013.

Finally, the Special Activity Airspace (SAA) dataset comes from NASA Sherlock data warehouse. It contains the start/ stop time, facility, type and altitude restrictions of each activity. We merged the SAA dataset with the facility geometry file provided by FAA National Flight Data Center (NFDC) and excluded those SAAs with unknown geometries.

3. METHODOLOGY

Using the data sources described above, we create a pooled, cross-sectional data set of flights across 97 airport pairs that took place in the year 2013. Following *(3)*, we characterize each flight by considering a nominal route rather than the actual flown trajectory. This is because one of the main sources of the flight inefficiency comes from reroute or detours to avoid adverse conditions. For example, a flight from LAX to JFK may take a long route crossing the Great Lakes because of unfavorable wind and weather conditions on the great circle route. In other words, it is the meteorological/ TMI condition on the most efficient route that "causes" the actual flight route. In this paper, we consider a single nominal route for each airport pair. The routes used in this paper are synthetic 4D great circle trajectory (GCT), which is theoretically the "most" efficient route, in terms of HIE[1], for each flight. As will be shown, by matching the synthetic GCT with features such as weather and MIT, we relate the flight HIE with different causal factors and provide an approach to quantifying how those factors impact HIE.

3.1 Generating Synthetic 4D Great Circle Trajectories

Generating 2D (longitude and latitude) great circle trajectory can be achieved by using spherical trigonometry and assuming the earth is an oblate ellipsoid. A realistic 4D great circle path, however, needs to satisfy the following two conditions: (a) it must have a reasonable altitude profile; (b) the time profile should not violate the basic law of kinematics. In this study, therefore, we first use WGS-84 ellipsoid and generate equally spaced waypoints. Then for each waypoint, we calculate the distances away from the origin and destination airports. Lastly, we use the historical flight trajectory dataset to approximate the altitude and time along the GCT by finding k-nearest neighbors based on the two distances. The full algorithm *GCT-Generator* is shown below.

[1] This is true without considering the exit/ entry points of the terminal.

TABLE 1 GCT-Generator Algorithm

Algorithm 1. GCT-Generator
Inputs: a. Historical flight track dataset: Track point: $TP_t^i = (lon_t^i, lat_t^i, alt_t^i, spd_t^i)$, with subscript t are time and superscript i as the i^{th} flight. Trajectory dataset with M flights: $FT = \{[TP_1^1, \dots, TP_{T_1}^1], \dots, [TP_1^M, \dots, TP_{T_M}^M]\}$. b. Coordinates of departure airport and arrival airport: $(lon_{dep}, lat_{dep}), (lon_{arr}, lat_{arr})$. Parameters: a. Space interval for the synthetic great circle trajectory (default 10 nautical miles): d. b. Number of nearest neighbors (default 50): K. Outputs: The synthetic 4D great circle trajectory.
Step 0: Random sample 75% of the total flights from FT. Get FT_s **Step 1**: Augment each TP_t^i in FT_s by calculating the great circle distance away from the origin airport and destination airport, respectively. Get $TP_t^i = (lon_t^i, lat_t^i, alt_t^i, spd_t^i, gcd_{ori,t}^i, gcd_{des,t}^i)$. **Step 2**: Build a 2D *kd-tree* based on $[(gcd_{ori,t}^i, gcd_{des,t}^i)]$ for $\forall i, t$. Get $tree_{GC}$. **Step 3**: Generate a 2D great circle trajectory given (lon_{dep}, lat_{dep}), (lon_{arr}, lat_{arr}) and d. Calculate $gcd_{ori,t}$ and $gcd_{des,t}$ for every waypoint. Get $GCT_{2D} = \{WP_i = (lon_i, lat_i, gcd_{ori,i}, gcd_{des,i}), \forall i\}$. **Step 5**: Query the $tree_{GC}$ with the two distance measures from GCT_{2D} and return K nearest points for every waypoint along GCT_{2D}. Get $QNP = \{QP_i = (TP_i^1, TP_i^2, \dots, TP_i^{50}), \forall i\}$. **Step 6:** For a waypoint WP_i in GCT_{2D}, weighted average the *altitudes* and *speeds* among the 50 queried points in QP_i, where the weights are linearly inverse proportional to the distance. Get $GCT_{2D} = \{WP_i = (lon_i, lat_i, gcd_{ori,i}, gcd_{des,i}, alt_i, spd_i), \forall i\}$. **Step 7:** For each WP_i, use (lon_i, lat_i, spd_i) and $(lon_{i-1}, lat_{i-1}, spd_{i-1})$ to calculate the time interval t_i. Return $GCT_{4D} = \{WP_i = (lon_i, lat_i, alt_i, t_i), \forall i \in [1, T]\}$.

3.2 Matching

To understand how weather, wind, TMIs and SAA affect flight en route inefficiency, we need to construct representative metrics for each flight based on the appropriate nominal route, which is the synthetic 4D great circle route described in Algorithm 1, but with the actual flight departure time. In other words, we want to characterize the conditions a given flight would have encountered if it had flown the nominal route. The detailed matching algorithms are introduced in the sections below.

3.2.1 Matching with convective weather and wind

Though convective weather and wind data come from different sources, their data structure is similar. Both can be stored in a fixed-dimension array, where the rows and columns are respectively the temporal and spatial indices, and planes are the fields of the dataset. To be more specific, the temporal indices for the weather dataset can be represented as the number of hours

elapsed from a base time, e.g., 01/01/2013 01:00 will have the temporal index of 1 with respect to the base time 01/01/2013 00:00, therefore, we have $365 \times 24 = 8{,}760$ rows in the weather array for the year 2013. Similarly, the wind array has 1,460 rows since wind data are stored every 6 hours. The spatial indices are the location of the "reference" points, which are the fixed locations in the airspace. For the weather data, they are ground stations; for the wind data, they are 3D grid points. As a result, there are 1,763 and $17 \times 435 = 7395$ columns in the weather and wind array, respectively. Since the weather dataset has seven different weather types and the wind dataset has two wind speeds (southerly and westerly), the number of planes is respectively 7 and 2. Lastly, the elements in the array are the features we need to match with. As will be shown later, storing data as fixed-dimension arrays greatly boosts the matching procedure by making tree-based search possible.

Matching a trajectory with a numeric array can be achieved simply by greedily searching the rows and columns and find the closest element(s) for every track point. Realizing that both the spatial (columns) and temporal (rows) dimensions of the weather/ wind array are fixed, we can simply build *k-d* trees to further structure the datasets, and batch query the trees to find the nearest neighbors for different track points. The algorithms are described in TABLE 2.

TABLE 2 Matching with Fixed-Dimension Array

Algorithm 2. Matching with fixed-dimension array
Inputs: a. Synthetic 4D great circle trajectories: $GCT_{4D} = \{WP_i = (lon_i, lat_i, alt_i, t_i), \forall i \in [1, T]\}$. b. Flight event dataset: $FE = \{[DepTime_i, AchDist_i, Inefficiency_i], \forall i \in [1, N]\}$. c. Fixed-dimension array with features: FDT. Parameters: a. Base time (default 01/01/2013 00:00:00 UTC): $baseT$. Outputs: Matched feature vectors.
Step 0: Convert all geographic coordinates from (lon, lat, alt) to Earth-centered rotational coordinates (x, y, z). **Step 1**: Construct great circle trajectories for all flights in the FE data by adding to the temporal dimension the difference between departure time $DepTime$ and base time $baseT$, while keeping the spatial dimension fixed. Get $FGCT = \{[WP_i^1, \forall i], \ldots, [WP_j^N, \forall j]\}$, where $WP_i^k = (x_i^k, y_i^k, z_i^k, elapT_i^k)$ is the i^{th} waypoint of the k^{th} flight. **Step 2**: Construct two *kd-trees* for spatial (s_tree) and temporal b (t_tree) dimensions, repectively. The spatial tree is built based on the location of the reference points (x, y, z), and the temporal tree is built based on the elapsed time from a base time $baseT$. **Step 3**: Query[1] s_tree with the converted coordinates (x, y, z) from $FGCT$, and t_tree with the elapsed time $elapT$ from $FGCT$. Get the tuple of the nearest spatial-temporal indices and return the corresponding elements from the feature array FDT. **Step 4**: If FDT is the wind array, then for each waypoint WP_t^k on flight k, we used the azimuth θ and matched southerly wind speed u_t^k and westerly wind speed v_t^k to calculate the headwind/ tailwind speed by $HTW_t^k = u_t^k cos\theta + v_t^k sin\theta$. Calculate the average HTW_t^k along the flight. For flight k, use the ground speed spd_t^k and HTW_t^k to calculate the airspeed, then calculate the distance

traveled with respect to the air (equivalent still air distance) WD^k.

Step 5:

If FDT is the weather array, then for each waypoint WP_t^k on flight k, we get a list of matched weather variables $MI_{t,m}^k$, where m represents one of the weather phenomenon, and a list of distances away from matched weather stations (MSD_t^k) to WP_t^k.

Compute the weighted average $MI_{t,m}^k$ and get weather scalar $MW_{t,m}^k$ for waypoint WP_t^k, where the weights are inversely linear proportional to the elements in MSD_t^k. Average $MW_{t,m}^k$ along all waypoints for flight k and return this metric.

Note:

1. For wind array, we performed nearest neighbor query, i.e., only return indices with the nearest distance; for weather array, we performed radius query, i.e., return all indices within a circle with radius *r*.

3.2.2 Matching with TMIs and SAA

MIT, AFP, MA and SAA all have similar structures, including a start time, a stop time, a location, and how it would affect the traffic. To be more specific, a typical MIT is recorded as $[st, et, reqfac, provfac, nas\_elem, alt, value]$, which can be interpreted as facility $reqfac$ (e.g., ZLA) requests a MIT to meter traffic into that facility, while facility $provfac$ (e.g., ZOA) implements a MIT restriction that is enforced at the NAS element (e.g., BTY) with value $value$ (e.g., 15 miles) and altitude range specified by alt from time st to time et. AFP, MA and SAA, similarly, can be represented as $[st, et, facility, alt, value]$, where $value$ for AFP includes average assigned delay and average acceptance rate; $value$ for MA is the alert type (red or yellow); and $value$ for SAA is the SUA type. To match with a TMI or SAA, a flight trajectory must satisfy the following condition: (a) it must crosses the corresponding facilities in a correct order, for example, a flight could match a MIT if it first crosses $provfac$, and then $reqfac$ and nas_elem; (b) the crossing time must within the period of st and et; (c) the crossing altitude must satisfy alt restrictions. TABLE 3 summarize the general matching framework.

TABLE 3 Matching with TMI/SAA

Algorithm 3. Matching with TMI/ SAA
Inputs: a. Synthetic 4D great circle trajectories: $GCT_{4D} = \{WP_i = (lon_i, lat_i, alt_i, t_i), \forall i \in [1, T]\}$. b. Flight event dataset: $FE = \{[DepTime_i, AchDist_i, Inefficiency_i], \forall i \in [1, N]\}$. c. TMI (SAA) dataset: $TSD = \{[st_i, et_i, facility_i, alt_i, value_i]\}$ Parameters: a. Buffer altitude (default 1000 ft): B_{alt}. b. Buffer NAS element radius (only applicable for MIT, default 0.5°): B_{nas}. Outputs: Matched feature vectors.
Step 0: Construct great circle trajectories for all flights in the FE data by adding to the temporal dimension the difference between departure time $DepTime$ and base time $baseT$, while keeping the spatial dimension fixed. Get $FGCT = \{[WP_i^1, \forall i], \dots, [WP_j^N, \forall j]\}$, where $WP_i^k = (lon_i^k, lat_i^k, alt, elapT_i^k)$ is the i^{th} waypoint of the k^{th} flight. **Step 1**: Filter TSD whose et is before the departure time $DepTime_i$ and st is after the arrival time of flight i. The remaining TSD_{filter} are retained as a candidate. **Step 2**:

Intersect flight i's great circle trajectory $FGCT_i$ with every candidateTSD_{filter}.
If TSD is MIT, then if $FGCT_i$ intersects the MIT_i's influencing area[2], $reqfac_i$ and $provfac_i$ in a correct order, and the time of intersecting with influencing area is within $[st_i, et_i]$, then go to Step 3, otherwise discards MIT_i.
Otherwise, if $FGCT_i$ intersects the $facility$, and the time of intersecting is within $[st_i, et_i]$, then go to Step 3, otherwise discards TSD_i.
Step 3:
If the altitude(s) of the intersecting waypoint(s) is within the altitude restriction $alt \pm B_{alt}$[3], add the records TSD_i to the matching list, otherwise discards TSD_i.
Step 4:
Count the number of matched TMIs/ SAA as $Count$.
If TSD is MIT, then calculate average and maximal of the matched MIT value, MIT duration and MIT stringencies[1].
If TSD is AFP, then calculate average and maximal of the matched average AFP assigned delay, maximal AFP assigned delay, and average AFP acceptance rate[4].
If TSD is MA or SAA, then calculate the average/max traverse time within the alert/SUA facility.
Return $Count$ and other calculated statistics.

Note:
1. MIT stringency is defined as the product of MIT value and MIT duration
2. If the NAS element is a fix, then the influencing area is a circle of radius B_{nas} around the fix. If the NAS element is a jet route, then the influencing area is swath centered on the jet route with overall width of B_{nas}. If the NAS element is a center/TRACON, then the influencing area is the polygon itself.
3. If alt is already specified as a range (e.g., ceiling and floor), then we don't add the B_{alt} to alt.
4. If a flight does not cross any AFPs, we set the AFP acceptance rate to be 999/hr.

Through Algorithms 2 and 3, we construct a panel data set within which each flight has a list of explanatory variables in the form of $X_{i,j} = [weather_i, wind_i, MIT_i, \dots, OD_{ij}]$, where index i indicates the i^{th} flight, and index j indicates the j^{th} airport pair. The description of the full explanatory variables is listed in TABLE 4.

TABLE 4 Summary Statistics of All Variables

Notation	Description	Min	Max	Mean
InEff	Flight en route inefficiency (in percentage)	0.0021	402.74	3.22
TS	Thunderstorm exposure (in percentage)	0.00	7.40	0.40
Rain	Rain exposure (in percentage)	0.00	20.60	2.37
Squall	Squall exposure (in percentage)	0.00	2.34	0.0027
Ice	Ice exposure (in percentage)	0.00	2.44	0.0043
Precipitation	Precipitation exposure (in percentage)	0.00	2.30	0.0055
Shower	Shower exposure (in percentage)	0.00	1.28	0.0072
Hail	Hail exposure (in percentage)	0.00	0.82	0.00027
AvgWindSpd	Average wind speed (positive if tailwind and negative if headwind) along the great circle route (in 100 m/s)	-0.39	0.39	0.0095
WindDist	Distance traveled with respect to air (equivalent still air distance, in 1000 nmi)	-0.29	0.23	-0.0050
NumMIT	Number of MIT crossed	0	13	0.32
MaxMITSTR	Maximal MIT stringency among all crossed MITs (in $100\ mile \cdot hr$)	0.00	9.83	0.18
NumAFP	Number of AFP crossed	0	2	0.02
MaxAFPDly	Maximal AFP assigned delay among all crossed AFP (in hours)	0	0.03	0.0002
MaxAFPArr	Maximal AFP acceptance rate among all crossed AFP (in 100	0	1.76*	0.013*

	per hour)			
NumSAA	Number of SAA crossed	0	9	0.57
MaxSAAT	Maximal transverse time within crossed SAA (in hours)	0	0.46	0.025
NumMARed	Number of red MA crossed	0	8	0.10
NumMAYel	Number of yellow MA crossed	0	5	0.013
MaxMAT	Maximal transverse time within crossed MA (in hours)	0	1.29	0.021
AchDist	Achieved distance (in 100 nmi)	0.56	26.64	6.91

*Note: * These are respectively the "true" maximal and average AFP acceptance rate after excluding all records with rate of 999/hr.*

3.3 Multiple Regression

We estimate linear models to investigate how meteorological conditions, TMIs and SAA on the great circle route affect flight HIE. In the regression model, the dependent variable is the flight en route inefficiency, and there are five categories of explanatory variables. The first category includes weather-related variables, such as thunderstorm, rain, ice and squall. Although there are seven types of weather events in our dataset, most of these occur only at low altitude and thus are unlikely to affect the en route phase of a flight. Therefore, we only include thunderstorm and squall events in the model specification. Since a flight may need to adjust its route to avoid the convective weather, we expect these variables to have positive effects on en route inefficiency. The second category includes wind-related variables – average tailwind speed (negative if headwind) and equivalent still air distance. Since flights in general favor strong tailwind, we expect higher tailwind speed to decrease and greater equivalent still air distance to increase HIE. The third category includes airport pair fixed effects; we fit the model with airport-pair specific intercepts and expect flights between pairs that are more inefficient (e.g., short haul flights) will have larger positive effects. The fourth category contains the TMIs and SAA. Like weather, we expect they will have positive effects to inefficiency. Finally, we include the achieved distance of each flight. When airport pair fixed effects are controlled, this variable mainly captures the effect of inefficient terminal entry and exit points and we expect it to have a positive impact on HIE. The model specification can be written as Equation 2, where index i represents the i^{th} flight, and index j represents the j^{th} airport pair.

$$\begin{aligned} 100 \cdot InEff_{i,j} = {} & \beta_j + \beta_1 \cdot TS_i + \beta_2 \cdot Squall_i + \beta_3 \cdot AvgWindSpd_i + \beta_4 \cdot WindDist_i + \beta_5 \\ & \cdot NumMIT_i + \beta_6 \cdot MaxMITSTR_i + \beta_7 \cdot NumAFP_i + \beta_8 \cdot MaxAFPDly_i + \beta_9 \\ & \cdot MaxAFPArr_i + \beta_{10} \cdot NumSAA_i + \beta_{11} \cdot MaxSAAT_i + \beta_{12} \cdot NumMARed_i \\ & + \beta_{13} \cdot NumMAYel_i + \beta_{14} \cdot MaxMAT_i + \beta_{15} \cdot AchDist_i \end{aligned} \quad (2)$$

To appropriately estimate the model, we must take into account the heteroskedasticity across different airport pairs. To verify such effect, we use Breusch-Pagan test and the results reject the null hypothesis of homoskedasticity against the alternative that the residual variances depend on the explanatory variables. Moreover, we expect autocorrelation for flights departing at similar times between the same airport pairs, since they may experience similar meteorological conditions or TMIs throughout the flights. We use the Wooldridge test and the results reject the null that there is no autocorrelation. Therefore, we estimate the final model using ordinary least squares (OLS) with Newey-West standard errors with a maximal lag of 2.

4. Results

To save space, TABLE 5 only reports the estimates of factors that interest us the most – weather, wind, TMIs and SAA – for four linear models. Model I, which we term "full model", includes all variables of interest and airport-pair fixed effects and is presented in the first column of TABLE 5. Model II, in which variables (except fixed effect variables) that are not significant at the 10% level are omitted, is presented in the second column. Model III, which eliminates the achieved distance effect, and Model IV, which eliminates the airport-pair fixed effects but includes a generic intercept and achieved distance, are presented in the last two columns of TABLE 5.

The vast majority of the estimates for the three reduced models (model II – model IV) are significant with expected signs. First of all, the estimates of thunderstorm confirm that convective weather along the great circle route increases the en route inefficiency. However, Model II and III have far smaller magnitude comparing with Model IV due to the inclusion of the airport-pair fixed effects – some direct routes inherently have more convective weather activities and therefore, much of the weather effects are absorbed by the airport-pair fixed effects. Secondly, tailwind speed on the great circle route seems to reduce inefficiency. When the airport-pair fixed effects are controlled, the negative estimates of average wind speed and positive estimates of equivalent still air distance imply that favorable tailwind conditions on the great circle route reduce flight inefficiency. This can be explained by the fact that flights prefer routes with higher tailwind speed, and therefore, if the great circle route has strong tailwind, flights gravitate toward routes close to the great circle, decreasing en route inefficiency. However, models in this study do not explicitly represent the mechanism of how winds affect the route choice; interested readers may refer to *(3)* and *(16)* for more discussions on winds and flight route choice. Thirdly, the estimates of MIT, AFP and SAA indicate that flights whose great circle routes have stronger MIT restrictions, AFP delays, and traverse time in the SUA areas are more inefficient than the others. We also notice that the estimates for all Monitor Alert associated variables are not significant. This is likely because an MA does not, per se, affect air traffic; rather it may result in a TMI such as an MIT or AFP, the effects of which are already incorporated in the model. Lastly, the estimates for achieved distance vary drastically depending on whether airport-pair fixed effects are included in the model. When airport-pair fixed effects are included (as in Model II), the estimate of achieved distance mainly derives from variation among flights within the same airport pairs; however, when there are no airport-pair fixed effects (as in Model IV), the estimate mostly captures the cross-sectional variation in achieved distance. Accordingly, the negative coefficient in Model IV indicates that long-haul flights tend to be more efficient; while the positive estimate in Model II indicates that for any particular airport pair, flights with longer achieved distance are more inefficient. Variation in achieved distance within a particular airport pair reflects variation in the efficiency of the entry and exit points; a higher achieved distance means these points are less efficient. The results in Models I and II therefore imply that flights with less efficient entry and exit points are also less efficient in the en route phase of flight. Figure 3, which further confirms the cross-sectional effects, presents the relationships between achieved distance and actual en route inefficiency, where scatter points with the same color represent flights between the same airport pair.

Figure 2 shows the airport-pair specific intercepts for Model II (red bars) and Model III (grey bars), where the x-axis shows the airport pairs ordered by the average achieved distance (left is shorter). Notice that Model II includes the variable $AchDist$, which varies marginally across flights between the same airport pair but differs drastically across different airport pairs. Therefore, in

Figure 2, we adjust Model II's airport-pair fixed effects by adding the product of coefficients before $AchDist$ and the average achieved distance for each airport pair. The estimates for both models are largely consistent with a decreasing trend to the right-hand side of the x-axis, indicating long-haul flights such as BOS to SFO are in general more efficient.

TABLE 5 Estimation Results

Variable	Models Est. / (Std.)			
	Model I	Model II	Model III	Model IV
constant	-	-	-	3.410*** (0.027)
TS	0.103*** (0.023)	0.109*** (0.021)	0.253*** (0.030)	0.819*** (0.030)
Squall	1.823 (1.377)	-	-	-
AvgWindSpd	-1.877*** (0.441)	-1.880*** (0.433)	-1.945*** (0.596)	-0.168 (0.113)
WindDist	6.775*** (1.415)	6.817*** (1.390)	6.247*** (1.872)	1.195*** (0.170)
NumMIT	0.148*** (0.016)	0.148*** (0.016)	0.314*** (0.027)	0.185*** (0.026)
MaxMITSTR	0.110*** (0.024)	0.110*** (0.024)	0.239*** (0.038)	0.244*** (0.040)
NumAFP	0.232 (2.004)	0.394*** (0.112)	1.078*** (0.224)	1.121*** (0.230)
MaxAFPDly	9.60 (14.393)	-	103.620*** (17.778)	112.215*** (18.050)
MaxAFPArr	-0.005 (0.212)	-	-	-
NumSAA	−0.003 (0.010)	-	-	-
MaxSAAT	2.666*** (0.271)	2.587*** (0.183)	2.816*** (0.242)	2.981*** (0.134)
NumMARed	-0.025 (0.018)	-	-	-
NumMAYel	-0.022 (0.028)	-	-	-
MaxMAT	0.086 (0.091)	-	-	-
AchDist	53.9478*** (1.871)	53.955*** (1.830)	-	-0.109*** (0.002)
Airport-pair fixed effect	…	…	…	-
Obs.	436,830	436,830	436,830	436,830
Adjusted R^2	0.654	0.654	0.445	0.040

Note: $* p < 0.1; ** p < 0.05; *** p < 0.01$

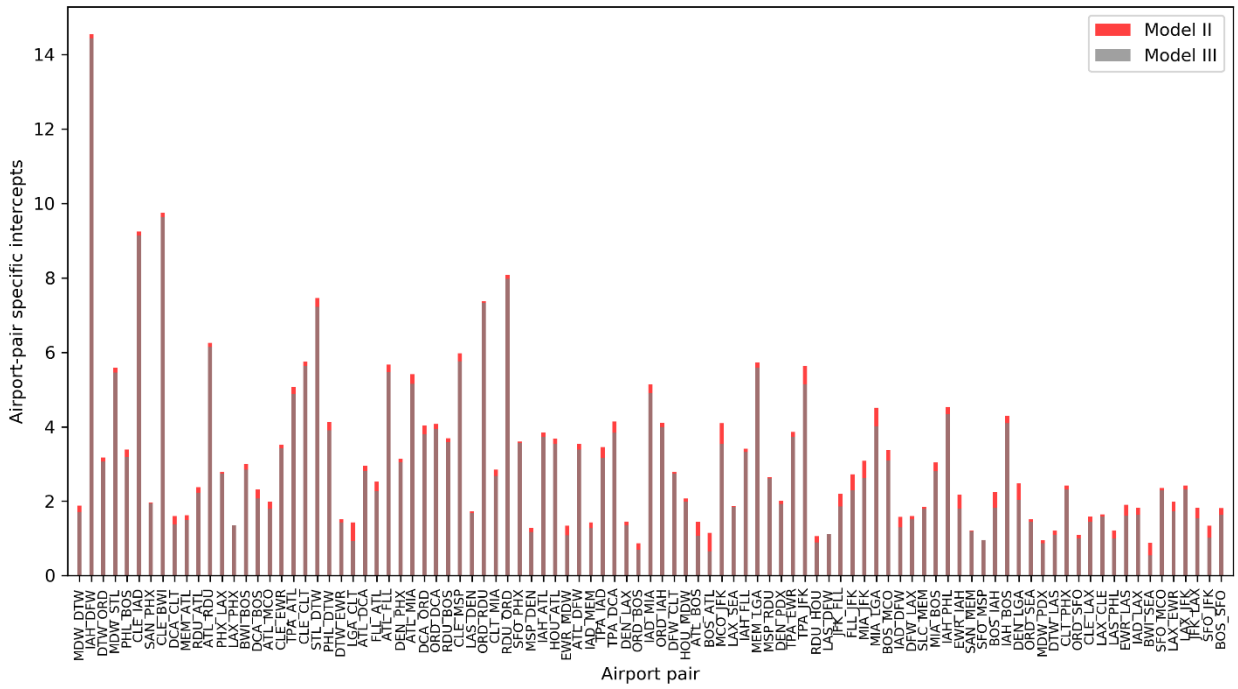

Figure 2 Airport-Pair Fixed Effects Estimation

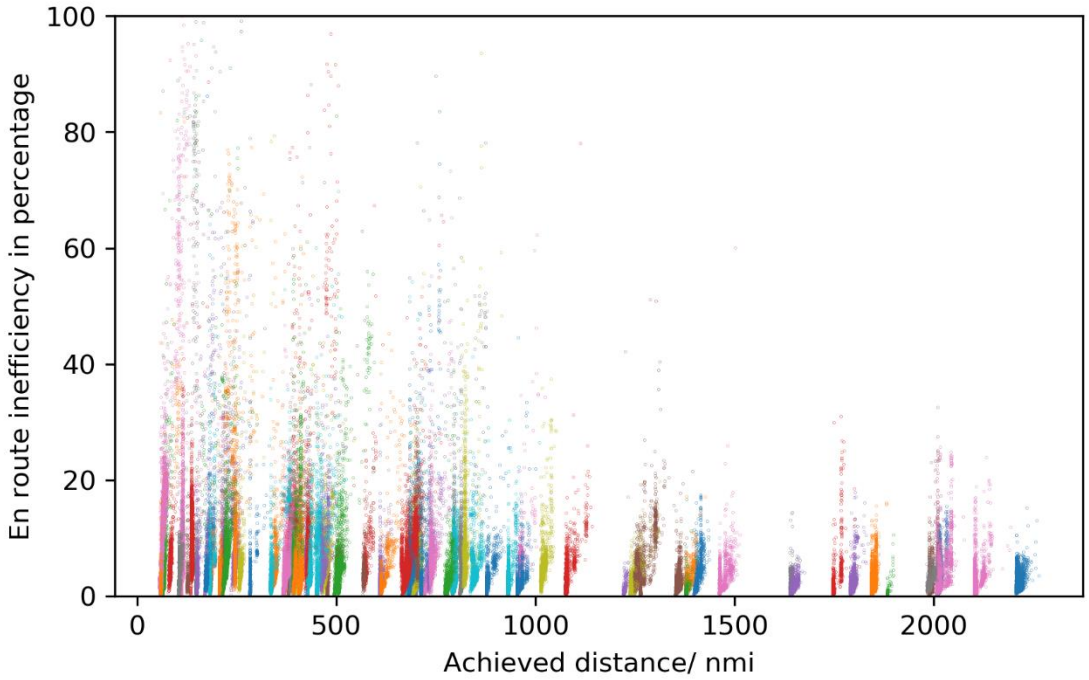

Figure 3 Achieved Distance vs HIE (HIE is truncated to 100)

5. Conclusions

As an extension to *(3)* and *(17)*, this study proposes econometric models to analyze flight en route

inefficiency, with emphasis on convective weather, wind, MIT, AFP, SAA and MA. We employ trajectory synthesis methods to generate hypothetical great circle trajectories for historical flights among 97 US airport pairs, and a trajectory matching framework to match those synthetic great circle routes with different factors (e.g., wind). Lastly, we develop metrics for the matched factors, and use multiple regression models with correction for heteroskedasticity and autocorrelation to quantitatively understand how they affect the flight en route inefficiency.

The proposed methods relate en route performance with different "causal" factors. Great circle routes are the "most" efficient routes by definition, and the meteorological and traffic conditions throughout the routes can be treated as proxies to how attractive the great circle trajectories would be. In the worst case where there is strong headwind, lots of convective weather, traffic management initiatives and SAAs, flights deviate from the great circle, and this increases inefficiency.

The estimation results, while confirm our conjectures, suggest that route structure is an important factor to en route inefficiency. Long haul flights, such as BOS to SFO, are in general more efficient than short haul flights. However, some airport pairs, even though they have similar distances, differ greatly in en route inefficiency. Examples include MDW to DTW (north) vs IAH to DFW (south), and SAN to PHX (west) vs CLE to BWI (east). Moreover, when airport-pair fixed effects are controlled, the achieved distance shows significant positive effect, indicating that inefficient terminal procedures will induce less efficient en route operations. The estimates for other covariates suggest that thunderstorm, MIT, SAA and AFP with longer assigned delays will increase the en route inefficiency, while strong tailwind on the great circle routes will reduce the inefficiency. Finally, the Monitor Alert does not appear to have much impact to en route inefficiency, which can be explained by the fact that the effect of MAs is mediated by TMI actions that are already incorporated in the model.

These models have several applications. First they can help target strategies to reduce HIE by predicting how changes the different factors that are subject to human control, such as TMIs and SAAs, would affect HIE. Second, it can be used to normalize comparisons between HIE in different times, regions, or airport pairs. As a specific example, from the fixed effects estimated in the model one can identify which airport pairs are the most and least HIE, all else equal. Pairs in the former group could then be further examined to improve their HIE.

Author Contribution Statement

The authors confirm contribution to the paper as follows: study conception and design: Yulin Liu, Mark Hansen; data collection: Mark Hansen, Yulin Liu; analysis and interpretation of results: Yulin Liu, Mark Hansen; draft manuscript preparation: Yulin Liu, Mark Hansen. All authors reviewed the results and approved the final version of the manuscript.

REFERENCES

1. EUROCONTROL. Performance Indicator – Horizontal Flight Efficiency. http://prudata.webfactional.com/wiki/images/a/a9/Horizontal_En_route_Flight_Efficiency_Methodology.pdf. Accessed Aug. 1, 2018.
2. Performance Review Commission and FAA-ATO. 2015 Comparison of Air Traffic Management-related Operational Performance: U.S./Europe. *European Commission. U.S. Department of Transportation*, 2016.
3. Liu, Y., M. Hansen, D. J. Lovell, C. Chuang, M. O. Ball, and J. M. Gulding. Causal Analysis of En Route Flight Inefficiency – the US Experience. *12th USA/Europe Air Traffic Management Research and Development Seminar (ATM2017), Seattle, WA, USA*, 2017.
4. McNally, D., K. Sheth, C. Gong, J. Love, C. H Lee, S. Sahlman, and J. Cheng. Dynamic weather routes: a weather avoidance system for near-term trajectory-based operations. *28th International Congress of the Aeronautical Sciences* 2012.
5. McNally, D., K. Sheth, C. Gong, P. Borchers, J. Osborne, D. Keany, B. Scott et al. Operational Evaluatioin of Dynamic Weather Routes at American Airlines, *10th USA/Europe Air Traffic Management Research and Development Seminar (ATM2013), Chicago, IL, USA,* 2013.
6. Federal Aviation Administration, Traffic Flow Management in the National Airspace System. https://www.fly.faa.gov/Products/Training/Traffic_Management_for_Pilots/TFM_in_the_NAS_Booklet_ca10.pdf. Accessed Aug. 1, 2018.
7. Girardet, B., L. Lapasset, D. Delahaye, C. Rabut. Wind-Optimal Path Planning: Application to Aircraft Trajectories. *13th International Conference on Control. Automation, Robotics and Vision, (ICARCV'14) Singapore,* 2014.
8. Palopo, K., R. D. Windhorst, S. Suharwardy, and H. Lee. Wind-optimal routing in the national airspace system. *Journal of Aircraft 47, no. 5*, 2010: pp. 1584-1592.
9. Sridhar, B., N. Y. Chen, K. N. Hok, O. Rodionova, D. Delahaye, and F. Linke. Strategic planning of efficient oceanic flights. *11th USA/Europe Air Traffic Management Research and Development Seminar (ATM2015), Lisbon, Portugal*, 2015.
10. Meyers, T. A., M. Klopfenstein, J. Mintzer, G. Wilmouth, and V. Sud. A preliminary analysis of the impact of miles-in-trail restrictions on NAS flight operations. *6th USA/Europe Air Traffic Management Research and Development Seminar (ATM2005), Baltimore, MD, USA*, 2005.
11. Tereshchenko, I., and M. Hansen. Relative Trajectory Cost Estimation for CTOP Applications Using Multivariate Nonparametric Finite Mixture Logit. *8th International Conference for Research in Air Transportation (ICRAT2018), Barcelona, Spain*, 2018.

12. Rock, D., and E. Sullivan. Negotiation automation for special use airspace. *Guidance, Navigation, and Control Conference and Exhibit*. 1999. p. 3991.
13. Krozel, J., N. Gaertner, J. Prete, and J. Torres. On-Demand Special Use Airspace. *The 26th Congress of ICAS and 8th AIAA ATIO*. 2008 p. 8938.
14. Hanson, K., J. Gulding, and A. Afshar. Analyzing the operational capacity effects of the monitor Alert parameter (MAP). *Integrated Communications Navigation and Surveillance (ICNS)*, 2016. pp. 6C1-1.
15. Estes, A. Airspace Flow Program Visualizer. http://math.umd.edu/~aestes/afp_visualizer_dev/. Accessed Aug. 1, 2018.
16. Liu, Y., M. Hansen, D. Lovell, and M. O. Ball. Predicting Aircraft Trajectory Choice -- A Nominal Route Approach. *8th International Conference for Research in Air Transportation (ICRAT2018), Barcelona, Spain*, 2018.
17. Hansen, M., Y. Liu, C. Chuang, D. Lovell, and M. O. Ball. *En Route Performance in the National Airspace System*. 96th Transportation Research Board Annual Meeting, Washington D.C., USA, 2017. https://trid.trb.org/view/1439676